7. R. Nowak, F. A. Schultz, M. Umana, H. Abruna, and R. W. Murray, *J. Electroanal. Chem., Interfacial Electrochem.*, **94**, 219 (1978).
8. F. B. Kaufman and E. M. Engler, *J. Am. Chem. Soc.*, **101**, 547 (1979).
9. N. Oyama and F. C. Anson, *ibid.*, **101**, 3450 (1979).
10. F. B. Kaufman, A. H. Schroeder, E. M. Engler, S. R. Kramer, and J. Q. Chambers, *ibid.*, In press.
11. F. B. Kaufman, A. H. Schroeder, E. M. Engler, J. Q. Chambers, and S. R. Kramer, Abstract 301, p. 778, The Electrochemical Society Extended Abstracts, Boston, Massachusetts, May 6-11, 1979.
12. P. Peerce and A. J. Bard, Abstract 302, p. 781, The Electrochemical Society Extended Abstracts, Boston, Massachusetts, May 6-11, 1979.
13. S. R. Rafikov, S. A. Pavlova, and I. I. Tverdokhlebova, "Determination of Molecular Weights and Polydispersity of High Polymers," Ch. IX, Daniel Davey and Co., Inc., New York (1964).
14. E. Laviron, *J. Electroanal. Chem. Interfacial Electrochem.*, **39**, 1 (1972).
15. N. Scott, N. Oyama, and F. C. Anson, *J. Electroanal. Chem. Interfacial Electrochem.*, In press.
16. T. P. DeAngelis, R. W. Hurst, A. M. Yacynck, H. B. Mark, Jr., W. R. Heineman, and J. S. Mattson, *Anal Chem.*, **49**, 1395 (1977).
17. K. Shimizu, T. Matsubara, and G. P. Sato, *Bull. Chem. Soc. Jpn.*, **47**, 1651 (1974).
18. J. Frank and G. S. Park, Editors, "Diffusion in Polymers," Chap. 10, Academic Press, New York (1968).
19. J. Frank and G. S. Park, Editors, "Diffusion in Polymers," Chap. 2-10, Academic Press, New York (1968).
20. L. Rebenfeld, P. J. Makarewicz, H. Weigmann, and G. L. Wilkes, *J. Macromol. Sci. Rev. Macromol. Chem.*, Chap. 15, p. 279 (1976).
21. R. McGregor, "Diffusion and Sorption in Fibers and Films," Chap. 15, Academic Press, New York (1974).
22. W. Rieman and H. F. Walton, "Ion Exchange in Analytical Chemistry," Pergamon, New York (1970).
23. H. Morawetz, "Macromolecules in Solution," 2nd ed., Chap. VII, John Wiley and Sons, Inc., New York (1975).
24. R. Kosfeld and L. Zumkley, *Ber. Bunsenges, Phys. Chem.*, **83**, 392 (1979).
25. H. Nishikawa and E. Tsuchida, *J. Phys. Chem.*, **79**, 2072 (1975).

A Digital Simulation Model for Electrochromic Processes at WO_3 Electrodes

Benjamin Reichman and Allen J. Bard*

Department of Chemistry, The University of Texas at Austin, Austin, Texas 78712

and Daniel Laser

Department of Chemistry, Tel Aviv University, Ramat-Aviv, Israel

ABSTRACT

Current-potential (i-E) curves for the electrochromic process at WO_3 electrodes were calculated with a digital simulation model which assigns the rate of charge transfer at the oxide/solution interface and the rate of diffusion of hydrogen into the bulk of the film as major variables. The simulated i-E curves agreed well with experimental ones for different types of WO_3 films and predicted the observed dependency of current on scan rate. The simulation required knowledge of the form of the electrochemical isotherm, which was obtained experimentally, and adjustment of a charge transfer rate constant, k_f, and the hydrogen atom diffusion coefficient within the film, D_H. The best fit was obtained with $k_f = 9 \times 10^{-3}$ sec^{-1} (mole/cm^3)$^{-2}$ and $D_H = 1 \times 10^{-9}$ to 2×10^{-10} cm^2/sec for the WO_3 films prepared by vacuum evaporation and $k_f = 7.2$ sec^{-1} (mole/cm^3)$^{-2}$ and $D_H = 5 \times 10^{-8}$ cm^2/sec for WO_3 anodic films. Simulated potential step results, which are similar to the experimental curves at longer times but show some discrepancy in the short time region, and concentration profiles are also reported.

Recently a great effort has been made to understand the electrochromic process which occurs at WO_3 electrodes during reduction and reoxidation and to construct display devices based on this process (1-5). While it appears clear that the process involves formation and oxidation of hydrogen tungsten bronzes, the detailed mechanism and a quantitative model of the electrochromic process and the steps which govern the rate of the color-bleach (CB) process have not been resolved. Different WO_3 films produced by vacuum evaporation exhibit different response times for coloring and bleaching, even when they are prepared by similar techniques (5). Moreover different types of WO_3 electrodes (*e.g.*, anodic *vs.* evaporated films) show significant differences in response time and electrochemical characteristics in the electrochromic region (6-8). The existence of water in the WO_3 film (7-9) and film porosity (7-8) appear to play important roles in determining the response time of the WO_3 electrodes. Crandall and Faughnan (10) discussed the factors entering into the dynamics of the CB process at WO_3 and compared values for the composition of the film with time, obtained during potential-step experiments, with calculated values. Their model assumed that mass transfer within the film was very large and that the rate-limiting steps involved proton transfer at the WO_3/liquid interface and the buildup of a "back emf" as the hydrogen bronze formed. Good agreement between the experimental and calculated values was obtained in the short time region after the start of the coloring step or when the coloring step was made at low potentials within the electrochromic region. With this model (5) the bleaching process is limited by the "space charge" which is created by accumulation of H^+ in the film. Arnoldussen (11) measured exchange currents and transfer coefficients for

* Electrochemical Society Active Member.
Key words: electrode, interfaces, films.

the electrochromic process but did not relate these values to any particular mechanism for the process. In the model previously suggested for the coloration process (10), diffusion of hydrogen atoms within the WO_3 film was not taken into consideration nor were fits to potential sweeps for different films attempted. These were thus restricted to descriptions of processes occurring at very short times after the start of the coloration process, at low coloration levels, or for very thin WO_3 films.

In this paper we present a digital simulation model of the WO_3 systems and report calculated current-potential (i-E) and current-time (i-t) curves which compare well to those obtained with WO_3 evaporated and anodic film electrodes in the electrochromic region (7, 8). This model includes the effects of charge-transfer from the electrode to the hydrogen ion in solution and diffusion of hydrogen atoms in the film. The differences in the electrochromic behavior between the evaporated and anodic film electrodes, which was attributed (7, 8) to a significant difference in the charge transfer rate constants and the diffusion coefficient of the hydrogen atom in both these films is demonstrated by the simulation. The model proposed here may also be relevant to the thin layer behavior found in electrodes prepared by coating with films of polymers or other electrodes with multilayer surface modification.

Models

Theoretical model.—The model we propose for the CB process at the WO_3 electrode is shown in Fig. 1. We assume that mass transfer of protons in solution and transport of electrons through the semiconducting films are not rate-limiting and that there is no barrier to electron injection at the metal/WO_3 contact (10). The rate-determining processes are then (i) charge transfer to protons at the WO_3/solution interface to form hydrogen atoms (H); (ii) diffusion of H-atoms within the film; (iii) build up of the H-atom concentration within the film towards the saturation level, y, determined by the ultimate film composition, H_yWO_3. This is represented by the equation

$$H^+ + e \underset{k_b}{\overset{k_f}{\rightleftharpoons}} H_i \xrightarrow{\text{diffusion}} H_b \qquad [1]$$

where H_i and H_b represent H-atoms at the interface and in the bulk film, and k_f and k_b are charge transfer rate constants. The concentration of H-atoms within the film, which is a function of x and t, is represented as [H] and the relative saturation or occupancy of H-atoms, θ, is given by

$$\theta = [H]/C_{max} \qquad [2]$$

where C_{max} represents the maximum concentration of hydrogen within the film. At the interface $[H] = [H]_i$ and $\theta = \theta_i$. The rate of formation of H-atoms at the interface can be related to the current density, j, and the potential drop across the interface, V, by the following equation

$$\frac{d[H]_i}{dt} = \frac{j}{n\mathbf{F}} - D\left(\frac{\partial^2[H]_i}{\partial x^2}\right) = k_f[H^+]C_{max}{}^q(1-\theta_i)^q \exp\left[\frac{-\beta n\mathbf{F}}{RT}V\right] - k_r C_{max}{}^m \theta_i{}^m \exp\left[\frac{(1-\beta)n\mathbf{F}}{RT}V\right]\exp[-r\theta_i] - D\left(\frac{\partial^2[H]_i}{\partial x^2}\right) \qquad [3]$$

This equation is of the usual form for interfacial charge transfer with a transfer coefficient, β. The empirical coefficients, q, m, and r, which must be determined experimentally, take account of the fact that: (i) the forward reaction is attenuated by a factor representing the availability of free sites on the WO_3 for H-atoms, $(1 - \theta_i)$; (ii) the backward reaction is governed by the activity of the dissolved hydrogen, rather than by its concentration [expressed by the term $\exp(-r\theta_i)$, which is equivalent to the interaction term in the Frumkin isotherm (12), where r is the factor expressing the extent of interaction between the absorbed hydrogen atoms, with a negative value of r implying a repulsive interaction].

We assume that the motion of hydrogen atoms in the film is governed by diffusion processes, governed by Fick's law (Eq. [4]), and that at the

$$\partial[H]/\partial t = D_H(\partial^2[H]/\partial x^2) \qquad [4]$$

boundaries of the film $x = 0$ (the oxide-electrolyte interface) and $x = l$ (the oxide-conductor interface) the conditions are always

$$\frac{j}{n\mathbf{F}} = D_H(\partial[H]/\partial x)_{x=0} \qquad (x = 0) \qquad [5]$$

$$D_H(\partial[H]/\partial x) = 0 \qquad (x = l) \qquad [6]$$

where D_H is the diffusion coefficient of hydrogen atom in the film. These boundary conditions express the assumptions that there is no accumulation of H-atoms at the oxide-electrolyte interface, and that there is no transfer of hydrogen across the oxide-conductor

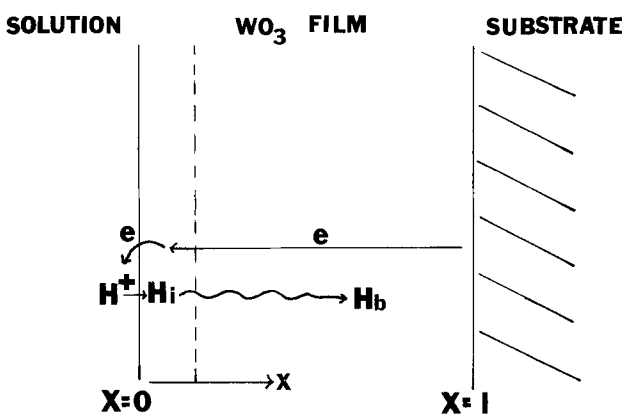

Fig. 1. Model for the electrochromic process at WO_3 electrodes

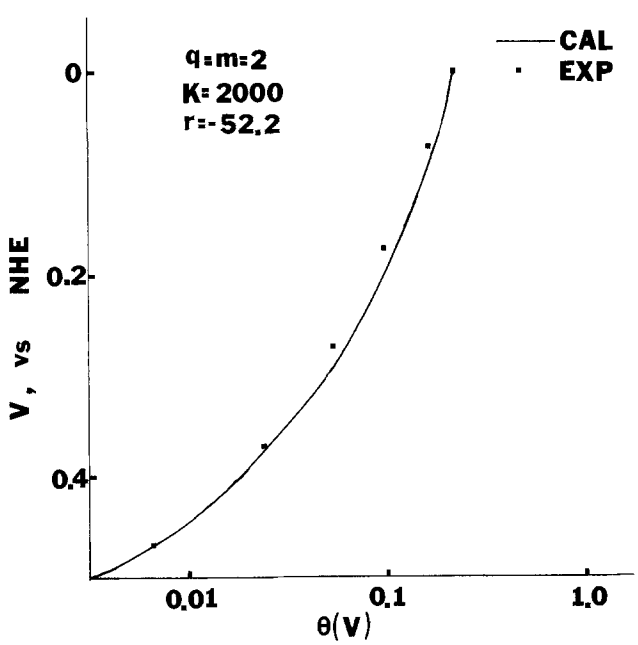

Fig. 2. Electrochemical isotherm for hydrogen in WO_3 electrodes. The line represents Eq. [9] with $q = m = 2$, $r = -52.2$, and $k = 2000$. The points are experimental data.

interface. The initial condition is

$$[H] = 0 \quad (t = 0, \quad \text{at all } x) \qquad [7]$$

Digital simulation model.—The digital simulation followed the usual finite difference approach to the solution of electrochemical problems (13-16), where the film was divided into increments of thickness, Δx, and [H] and θ are calculated for different times, divided into increments, Δt. The [H] (and θ) in the first space element (*i.e.*, at the surface) is obtained from its rate of production, Eq. [3], corrected for the loss into the film by diffusion. Within the film, [H] and θ are controlled only by diffusion, subject to the constraints of finite thickness and saturation of [H] at its maximum value at a given potential.

Results and Discussion

Hydrogen isotherm.—To carry out the simulation, values of the parameters q, m, and r must be obtained. These are available from the equilibrium isotherm. At a given potential, V, equilibrium is achieved when the distribution of H throughout the film is uniform (*i.e.*, $\partial\theta/\partial x = 0$) and θ attains its maximum value for that potential, $\theta_{eq}(V)$. At equilibrium, $j = 0$, so from Eq. [3]

$$k_f[H^+][1 - \theta_{eq}(V)]^q \exp[(-\beta n\mathbf{F}/RT)V] = k_r\theta_{eq}(V)^m \exp[(1 - \beta)n\mathbf{F}V/RT]C_{max}{}^{m-q}e^{-r\theta_{eq}(V)} \qquad [8]$$

$$\frac{\theta_{eq}(V)^m}{[1 - \theta_{eq}(V)]^q} e^{-r\theta_{eq}(V)} = K[H^+]\, e^{-(n\mathbf{F}/RT)V} C_{max}{}^{m-q} \qquad [9]$$

where $K = k_f/k_r$. C_{max} was evaluated by assuming a formula of HWO_3, for the oxide saturated with hydrogen (17). The parameters q, m, and r were estimated by fitting Eq. [9] to the experimental electrochromic isotherm. The isotherm was determined

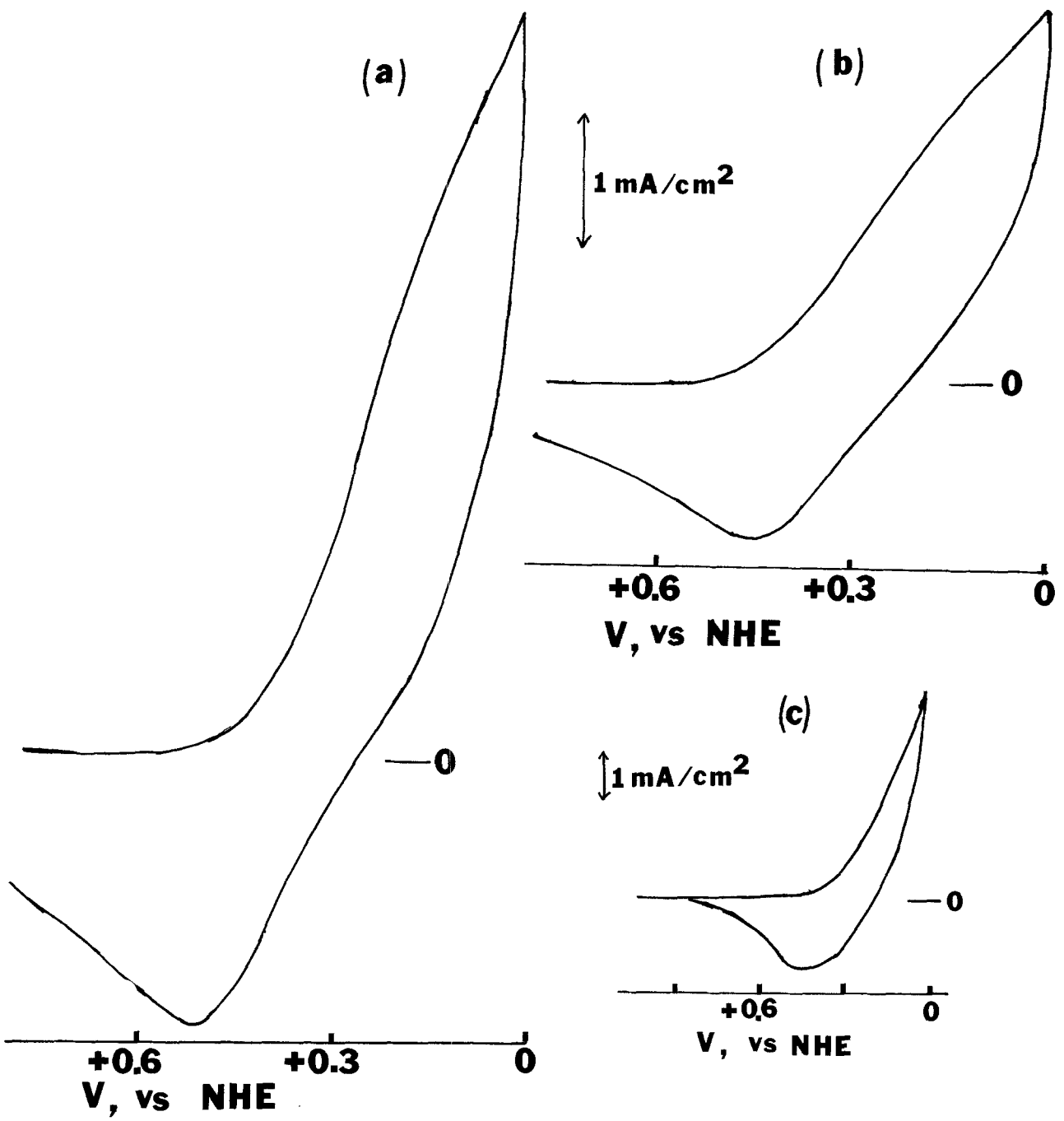

Fig. 3. Simulated current-potential curves for the electrochromic process at WO_3. Film thickness, 1.8 μm; scan rate, 100 mV/sec; k_f, 9×10^{-3} sec^{-1} (mole/cm^3)$^{-2}$; and (a) $D_H = 1 \times 10^{-9}$ cm^2/sec, (b) $D_H = 2 \times 10^{-10}$ cm^2/sec. (c) Typical experimental current-potential curve for WO_3 evaporated film electrode 1.8 μm thick at scan rate of 100 mV/sec.

by stepping the WO_3 electrode potential to a certain value, V, with respect to the reference electrode ($Hg/Hg_2SO_4/1M\ H_2SO_4$), within the electrochromic region. After stepping the potential, the amount of charge involved in coloration was determined coulometrically by integrating the current until it decayed to zero and equilibrium was attained. This procedure was repeated with various potentials within the coloration region. A similar isotherm was obtained by Faughnan *et al.* (17). The experimental isotherm and the calculated one are shown in Fig. 2. The best fit was obtained with $q = m = 2$, $K = 2000$ cm^3/mole, and $r = -52.2$. A similar conclusion regarding the values of q and m was reached by Faughnan *et al.* (17). Since $K = k_f/k_r$, the assignment of a numerical value to K requires that only the magnitude of either k_f or k_r is needed in the simulation.

Evaporated film electrodes.—The digital simulation was carried out by taking $\beta = 0.5$ and assuming different values for k_f and D_H. Typical simulated curves (illustrated with a 1 cm^2 electrode area, 1.8 μm thick film, and scan rate, v, of 100 mV/sec) with $k_f = 9 \times 10^{-3}$ sec^{-1} (mole/cm^3)$^{-2}$ and D_H of (a) 1×10^{-9} and (b) 2×10^{-10} cm^2/sec are shown in Fig. 3. These are of the same shape as experimental i-E curves found for evaporated film WO_3 electrodes (7) [Fig. 3(c)]. Thus the cathodic current, which begins at ~0.5V, increases monotonically upon scanning to more negative potentials and upon reversal of the scan direction, the current remains cathodic only becoming anodic at potentials 0.2-0.3V more positive than the reversal potential for 1.8 μm films. The anodic current peak is typically 2-3 times smaller than the cathodic current at 0V. The magnitudes of currents shown in the simulated curves are also similar to those obtained experimentally. The dependence of the simulated electrochromic i-E curves on scan rate is shown in Fig. 4. The simulation shows that the coloration current at more negative potentials is linearly dependent on $v^{1/2}$ as observed experimentally with the evaporated WO_3 film electrodes (7) [see Fig. 4(c)].

The k_f and D_H values both affect the rate of the electrochromic process, the shape of the i-E curves, and the scan rate dependence. For a film with a given thickness, l, the potential at which the simulated electrochromic current changes its sign from cathodic to anodic following the change in the direction of the potential scan, is very sensitive to the charge transfer rate constant, k_f. This is illustrated in Fig. 5. Typically the experiments with 1.8 μm WO_3 evaporated film electrodes produced i-V curves which crossed the X-axis about 200-300 mV after the potential of scan reversal. This behavior, shown in Fig. 3, puts k_f at a value of $\sim 9 \times 10^{-3}$ sec^{-1} (mole/cm^3)$^{-2}$. For a typical evaporated WO_3 film, this choice of k_f value produces a ratio of the cathodic to the anodic peak current similar to the experimental values. For some evaporated films the experimental anodic current started to appear at more positive potentials. The simulation results suggest that in these cases k_f was smaller, perhaps because of some change in the nature of the surface of the film. In other extreme cases the experimental anodic current started to appear at a more negative potential, indicating a larger k_f value for these. The value of D_H also affects the potential at which the anodic current begins on scan reversal but its effect on this value is smaller than that of k_f. However the magnitude of D_H strongly affects the size of the electrochromic current, as shown in Fig. 3. For two films with the same k_f an increase in D_H by a factor of five causes an increase

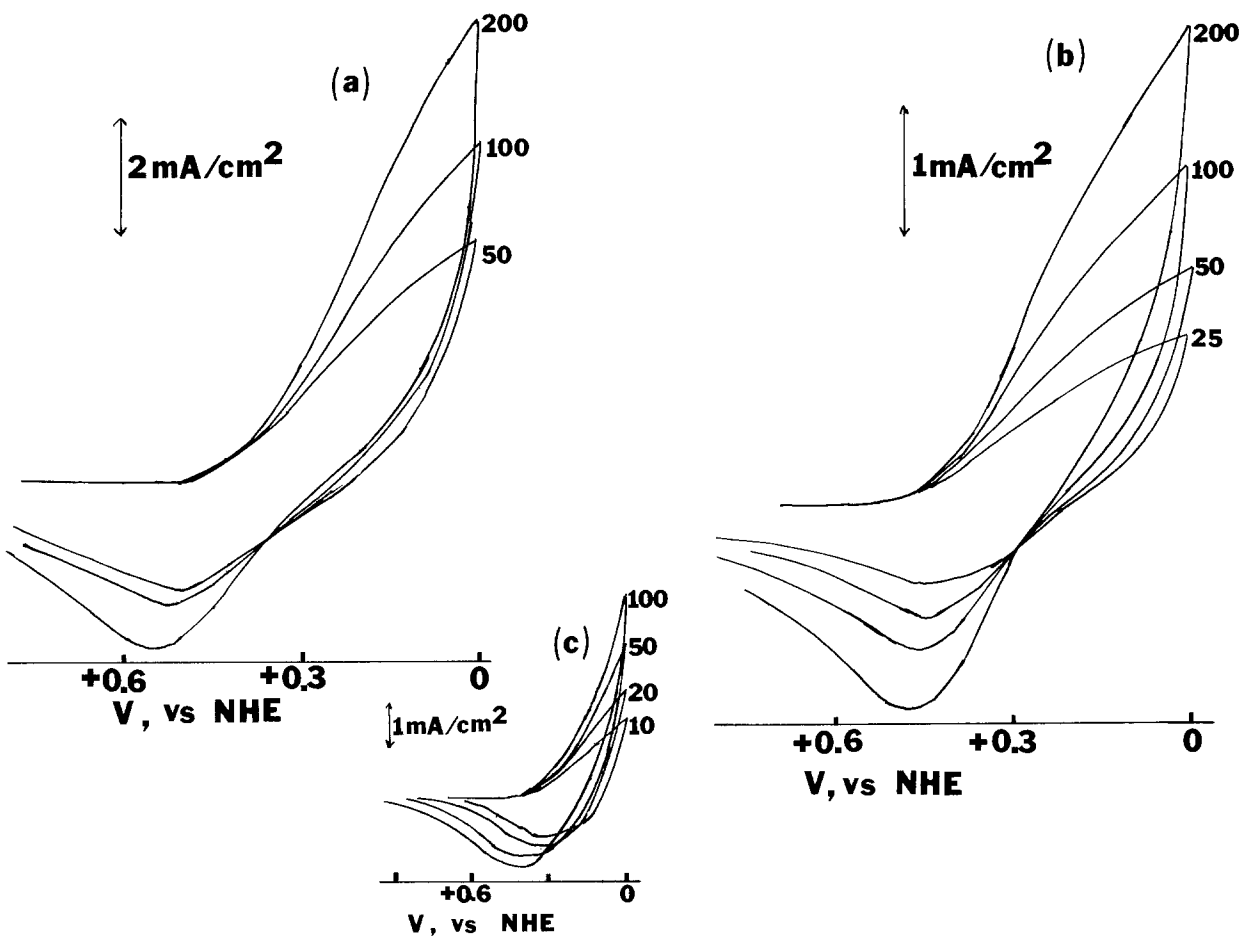

Fig. 4. (a), (b) Simulated electrochromic current-potential curves, as in Fig. 3, for different scan rates. (c) Experimental current-potential curve of the evaporated film shown in Fig. 3(c) at different scan rates. The numbers are the scan rates in mV/sec.

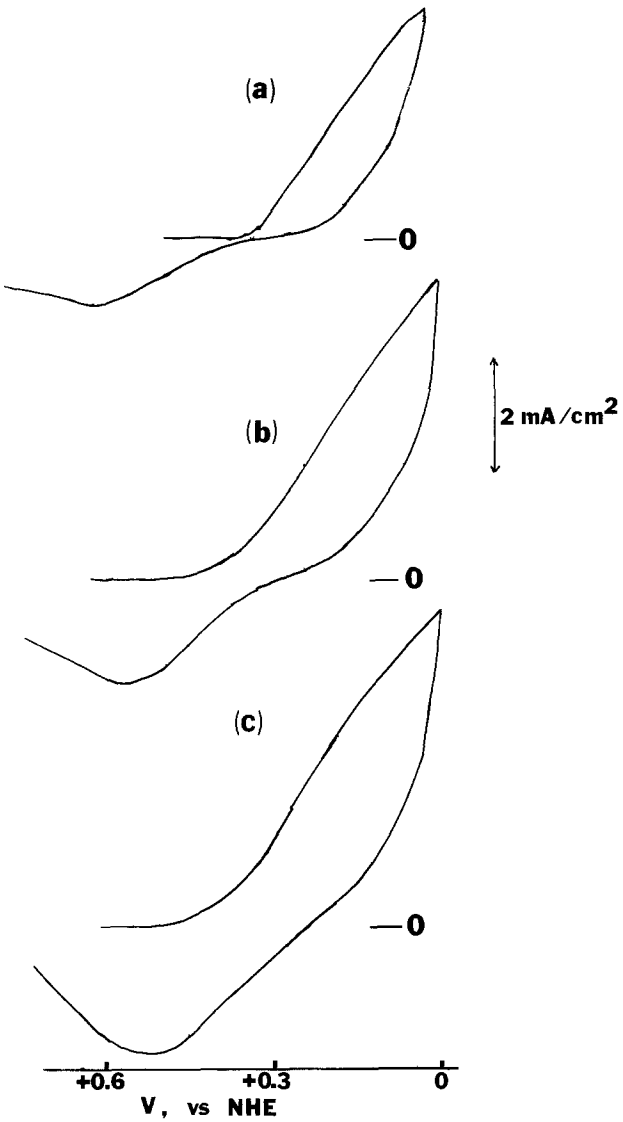

Fig. 5. Simulated current-potential curves for the electrochromic process at a WO_3 film, 1.8 μm thick with $D_H = 1 \times 10^{-9}$ cm^2/sec and with k_f values of (a) 1.8×10^{-3}, (b) 4.5×10^{-3}, (c) 9×10^{-3} sec^{-1} (mole/cm^3)$^{-2}$.

in the electrochromic current by a factor of about 2. The values of D_H which produced simulated i-E curves with currents similar in magnitude to typical experimental ones with evaporated WO_3 films were 1×10^{-9}-2×10^{-10} cm^2/sec. Mainly l and D_H determine the dependence of the current on the scan rate. The calculated concentration profile of the hydrogen atom within the evaporated film at the negative potential limit (0V *vs.* NHE) is shown in Fig. 6(a) and (b) for different scan rates and two different film thicknesses. As expected the concentration profile shows a sharp slope at the surface, which is caused by slow diffusion into the film. It is this behavior which results in the $v^{1/2}$ dependence observed in the i-E curves. We have observed similar i-E curves and scan rate dependences for WO_3 layers obtained by thermal oxidation of W (18), which suggests that these films have k_f and D_H values similar to those of the evaporated film electrodes.

Anodic film electrodes.—The shape of the i-E curves and the scan rate dependence were different for the WO_3 anodic film electrodes (7, 8) [Fig. 7(a) and (b)]. These i-E curves appear more reversible than those for the WO_3 evaporated film electrodes discussed above. Thus, the electrochromic current changes sign from cathodic (coloring) to anodic (bleaching) almost immediately after the direction of the potential scan is reversed. The anodic current magnitude is similar to that of the cathodic current and generally the curves look more symmetrical. Moreover, the electrochromic current in this case depends directly on v [Fig. 7(b)] as opposed to the $v^{1/2}$ dependence found with the evaporated or thermally oxidized films. This difference in behavior can be ascribed to large differences in k_f and D_H. Indeed to obtain simulated i-E curves which resembled those obtained experimentally with the WO_3 anodic film electrodes, much larger values of k_f and D_H had to be used [Fig. 7(c) and (d)]. To obtain an i-E curve of this shape, k_f must be taken as about 7.2 sec^{-1} (mole/cm^3)$^{-2}$. D_H values of about 5×10^{-8} cm^2/sec then yield current magnitudes in the simulated i-E curves similar to those obtained experimentally. With these k_f and D_H values, the current in the simulated i-E curves is linearly dependent on v [compare curves (b) and (d) in Fig. 7]. The H-concentration profile within the film, calculated for $E = 0$V *vs.* NHE, with the same thickness (l), k_f, and D_H values as in Fig. 7 is shown for several scan rates in Fig. 6(c). These concentration profiles are almost flat, so that the concentration of hydrogen atoms is essentially uniform throughout the film. This concentration is also near the equilibrium value at this potential (compare with the data in Fig. 2). This type of response is typical of "thin film" behavior as found for thin electrochemical cells (19) and as well as for adsorbed layers, modified electrodes, etc., and results in a dependency of current directly on v.

Current-time curves.—Simulated current-time (i-t) curves for the electrochromic process can be calculated with the same digital simulation model and parameters. Simulated i-t curves for the coloration process at two different potentials are compared to an experimental one obtained with the WO_3 evaporated films in Fig. 8. The values of k_f and D_H used for the calculation of the simulated curves are those which were used for calculated i-E curves of Fig. 3. While these values give simulated i-t curves which are similar to the experimental ones, there is some discrepancy between the simulated and the experimental curves in the shorter time region. In general the experimental i-t curves show a bump or irregularity in the short time region, while the simulated curves are smooth at all times. The source of this irregularity in the short time region has not yet been established, and we could not simulate it by any minor variations in the model (such as attempts to incorporate a proton source, like water, within the film). The H-concentration profiles during a coloration potential step, which are directly related to the intensity, were calculated for several times (Fig. 9). Such curves are useful for predicting what degree of coloration will be obtained at a given time after the onset of a potential step into the coloration region. For the evaporated film electrodes, 1.8 μm thick, 50% of the maximum coloration occurs at about 15 sec. This is similar to what is found experimentally.

Conclusions

The model suggested here describes in a satisfactory way the experimental results obtained for the electrochromic processes at different types of WO_3 electrodes. The model proposes as major factors both the rate of diffusion of hydrogen atoms within the WO_3 films and the rate of charge transfer at the WO_3/solution interface along with the saturation effect which occurs as the hydrogen tungsten bronze forms. The scan rate dependence of the current and rate of coloration of the films is mainly a function of D_H and l and the behavior can be roughly classified according to the dimensionless parameter $S = (RT/\mathbf{F})D_H/vl^2$. When S is greater than $\sim$1, i varies with v and "thin layer" behavior is observed. For S less than $\sim$0.1, a $v^{1/2}$ dependency is found. This model also describes in a generally satisfactory

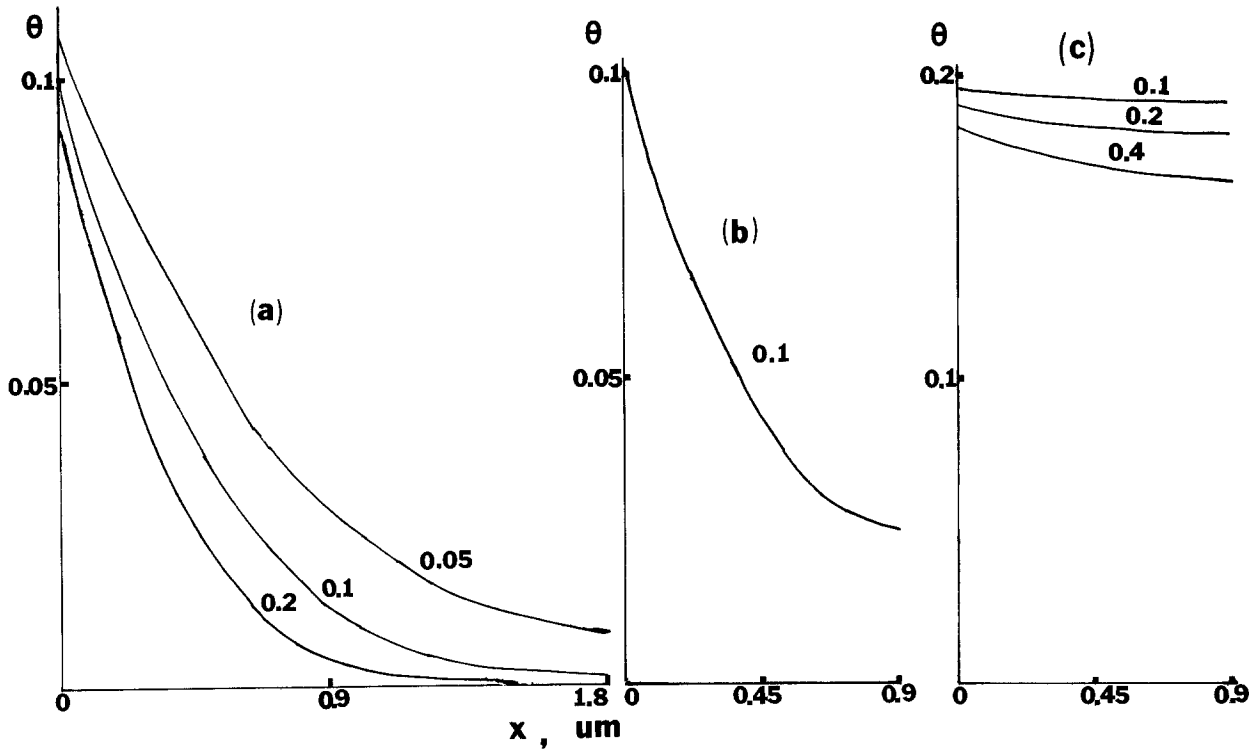

Fig. 6. Simulated concentration profiles of hydrogen atoms within the WO_3 evaporated film. (a) $k_f = 9 \times 10^{-3}$ sec^{-1} (mole/cm^3)$^{-2}$, $D_H = 1 \times 10^{-9}$ cm^2/sec, $l = 1.8$ μm; (b) as (a) with $l = 0.9$ μm; (c) $k_f = 7.2$ sec^{-1} (mole/cm^3)$^{-2}$, $D_H = 5 \times 10^{-8}$ cm^2/sec, $l = 0.9$ μm. All curves are for an electrode potential of 0V, at the scan rates indicated on the curves (mV/sec).

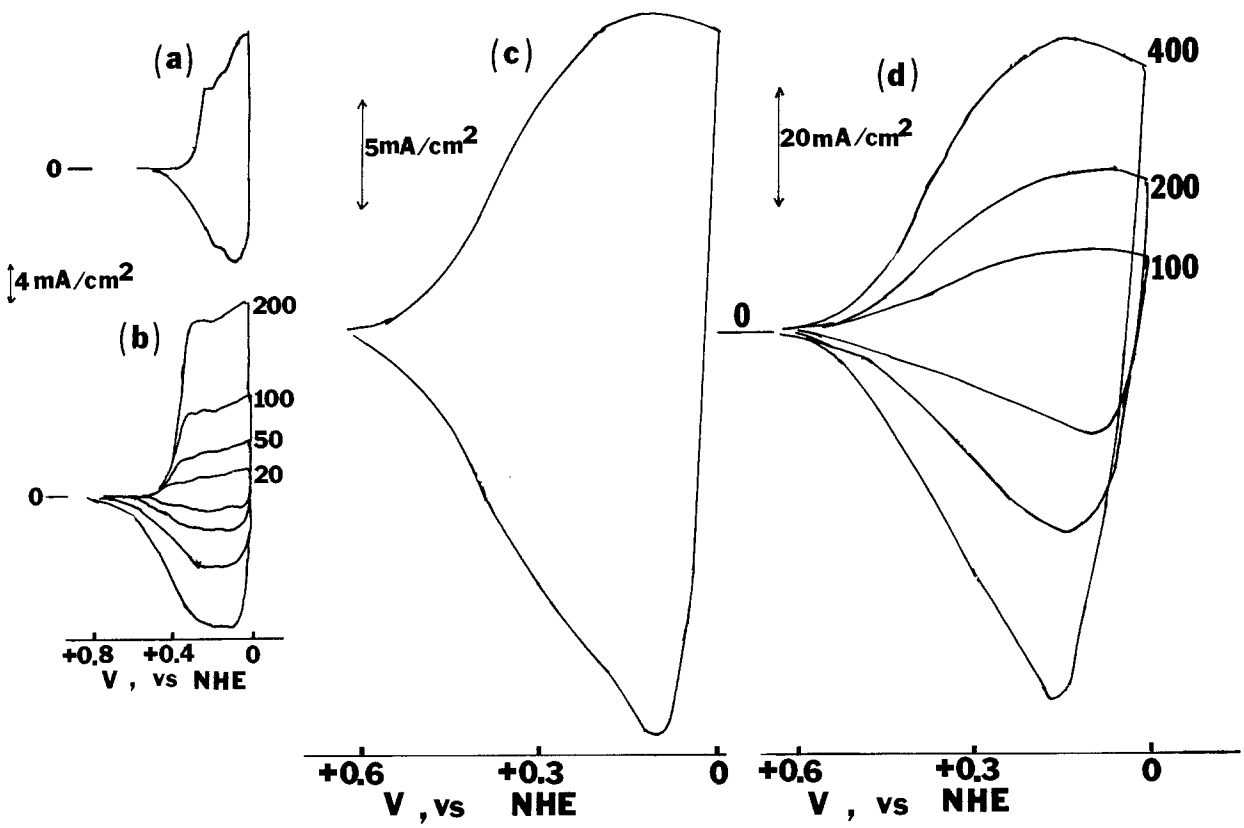

Fig. 7. (a) Experimental current-potential curves recorded at 100 mV/sec for 0.9 μm thick anodic film electrodes in 1M H_2SO_4 solution; (b) as (a) for different scan rates indicated on the curves (mV/sec); (c) simulated current-potential curve with $l = 0.9$ μm, $k_f = 7.2$ sec^{-1} (mole/cm^3)$^{-2}$, $D_H = 5 \times 10^{-8}$ cm^2/sec, scan rate = 100 mV/sec; (d) simulated current-potential curve as in (c), for different scan rates.

way the i-E behavior of WO_3 electrodes as well as i-t transients at longer times. The discrepancies between the experimental data and the simulated i-t curves in the short time region remain to be explained and modifications of the model which can simulate this behavior may lead to further insight into the nature of the electrochromic process and changes which occur in the films during coloration and bleaching.

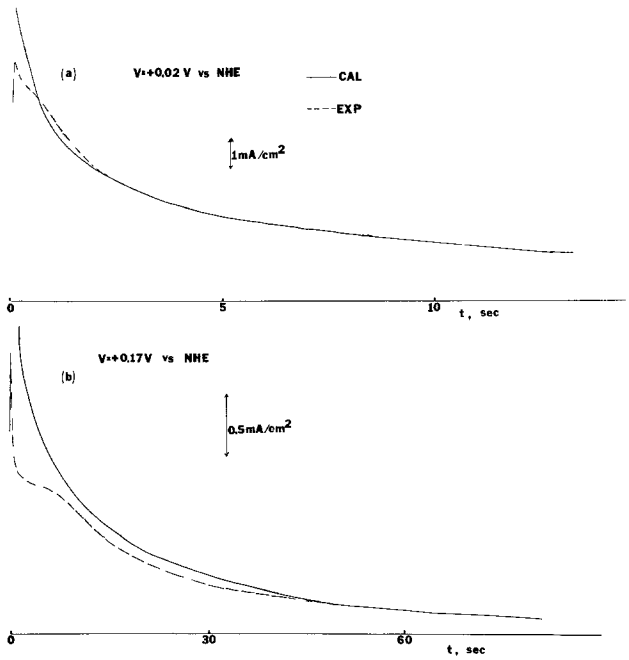

Fig. 8. Simulated (——) and experimental (- - -) current-time curves during the coloration process at WO_3 evaporated film electrode, 1.8 μm thick at two different potentials (a) +0.02V, (b) +0.17V *vs.* NHE. The values of k_f and D_H used for the calculation were the same as those which were used to calculate the current-potential curves of Fig. 3(a).

Acknowledgment

The support of this research by Texas Instruments is gratefully acknowledged.

Manuscript submitted July 25, 1979; revised manuscript received Aug. 29, 1979.

Any discussion of this paper will appear in a Discussion Section to be published in the December 1980 JOURNAL. All discussions for the December 1980 Discussion Section should be submitted by Aug. 1, 1980.

Publication costs of this article were assisted by The University of Texas at Austin.

REFERENCES

1. S. K. Deb, *Philos, Mag.*, **27**, 807 (1973).
2. B. W. Faughnan, R. S. Crandall, and P. M. Heyman, *RCA Rev.*, **36**, 177 (1975).
3. H. N. Hersh, W. E. Kramer, and J. H. McGee, *Appl. Phys. Lett.*, **27**, 646 (1975).
4. I. F. Chang, B. L. Gilbert, and T. I. Sun, *This Journal*, **122**, 955 (1975).
5. B. W. Faughnan, R. S. Crandall, and M. A. Lampert, *Appl. Phys. Lett.*, **27**, 275 (1975).
6. H. R. Zeller and H. U. Beyeler, *Appl. Phys.*, **13**, 231 (1977).
7. B. Reichman and A. J. Bard, *This Journal*, **126**, 583 (1979).
8. B. Reichman and A. J. Bard, Abstract B-9, The 20th Conference on Electronic Materials, University of California, Santa Barbara, Calif., June, 1978.
9. J. Hurditch, *Electron. Lett.*, **11**, 142 (1975).
10. R. S. Crandall and B. W. Faugnan, *Appl. Phys.*

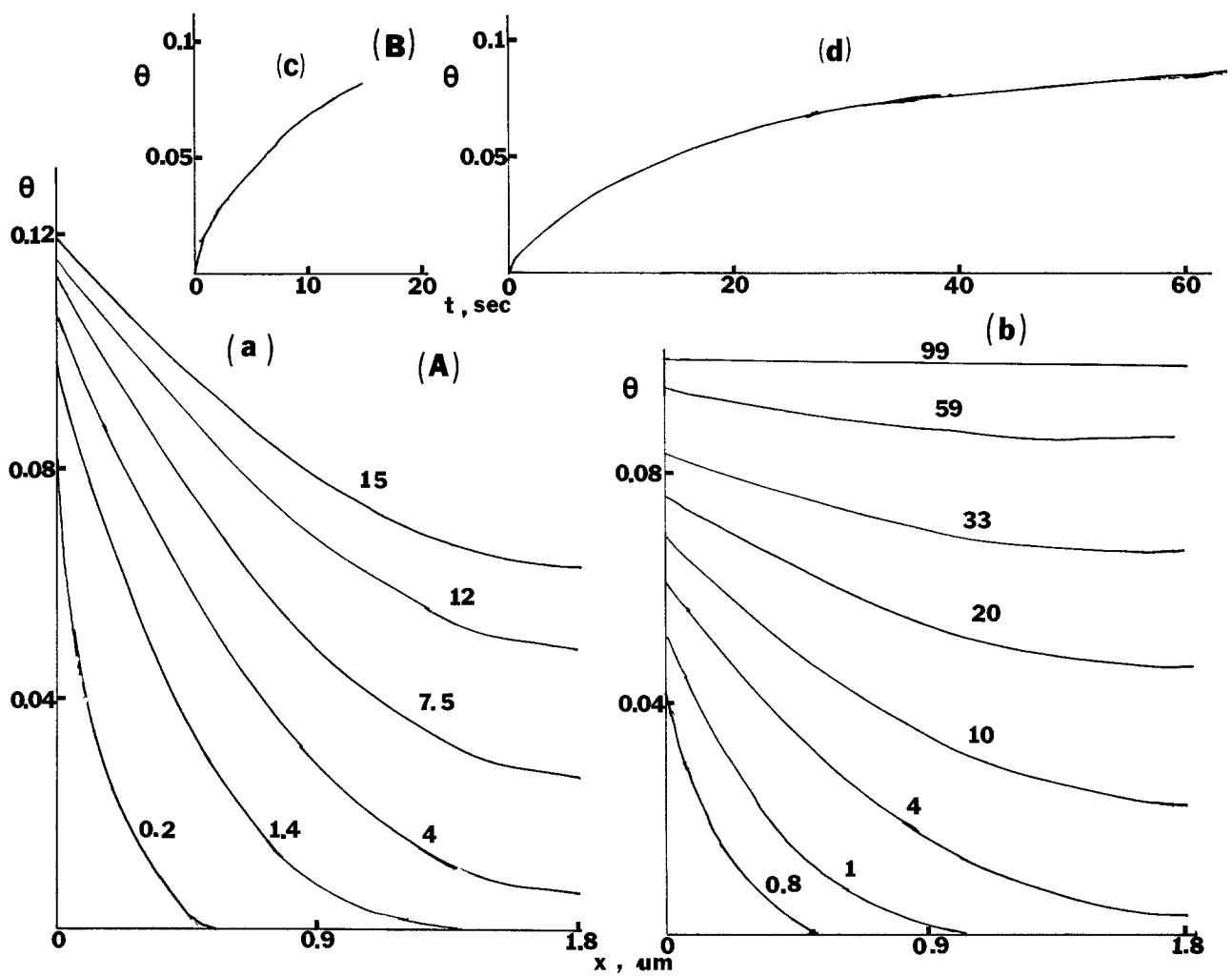

Fig. 9. (A) Calculated hydrogen concentration profiles at different times (sec) shown on curves during the coloration process at (a) $V = +0.02$V and (b) +0.17V (*vs.* NHE). (B) Calculated total hydrogen concentration inside the WO_3 film, as a function of time during the coloration process at (c) $V = +0.02$V (d) $V = +0.17$V (*vs.* NHE). The parameters k_f and D_H are those of Fig. 3(a).

Lett., **28**, 95 (1976).
11. T. C. Arnoldussen, Paper 199 presented at The Electrochemical Society Meeting, Las Vegas, Nevada, October 17-22, 1976.
12. E. Gileadi, E. Kirowa-Eisner, and J. Penciner, "Interfacial Electrochemistry," p. 83, Addison-Wesley, Reading, Mass. (1975).
13. S. W. Feldberg, in "Electroanalytical Chemistry," Vol. 3, A. J. Bard, Editor, Chap. 4, Marcel Dekker, Inc., New York (1965).
14. S. W. Feldberg, in "Computers in Chemistry and Instrumentation," Vol. 2, J. S. Mattson, H. B. Mark, Jr., and H. C. MacDonald, Jr., Editors, Chap. 7, Marcel Dekker, New York (1972).
15. A. J. Bard and L. R. Faulkner, "Electrochemical Methods," Appendix B, Wiley, New York (1980).
16. I. B. Goldberg, A. J. Bard, and S. W. Feldberg, *J. Phys. Chem.*, **76**, 2250 (1972).
17. R. S. Crandall, P. J. Wajtoneicz, and B. W. Faughnan, *Solid State Commun.*, **18**, 1409 (1976).
18. B. Reichman and A. J. Bard, *This Journal*, In press.
19. A. T. Hubbard and F. C. Anson, in "Electroanalytical Chemistry," Vol. 4, A. J. Bard, Editor, Chap. 2, Marcel Dekker, Inc., New York (1966).

The Thionine-Coated Electrode for Photogalvanic Cells

W. John Albery, Andrew W. Foulds, Keith J. Hall, and A. Robert Hillman

Department of Chemistry, Imperial College, London SW7 2AY, England

ABSTRACT

The successful operation of a photogalvanic cell for solar energy conversion requires that the illuminated electrode should discriminate between the two redox couples in solution. In the case of the iron-thionine system the electrode must oxidize photogenerated leucothionine but not reduce the photogenerated Fe(III). Modified electrodes with coatings of thionine of up to 20 monolayers can be prepared on Pt and SnO_2. These electrodes have been investigated using ring disk, cyclic voltammetry, XPES, and spectroelectrochemical measurements. Results for the modified electrode kinetics are presented for the following systems: thionine, disulfonated thionine, Fe(II), $Fe(CN)_6^{4-}$, $Ru(bpy)_3^{3+}$, Ce(IV), quinone, and N,N,N′,N′-tetramethyl-p-phenylenediamine. The results for the Fe(III) and thionine systems show that this modified electrode is suitable for the iron-thionine photogalvanic cell.

A typical photogalvanic cell for solar energy conversion is shown in Fig. 1. The iron-thionine system for such a cell works according to the following reaction scheme (1-3)

$$\mathrm{Th} \xrightarrow{h\nu} \mathrm{Th}^*$$

$$\mathrm{Th}^* + \mathrm{Fe(II)} \xrightarrow{H^+} \mathrm{S}^\cdot + \mathrm{Fe(III)}$$

$$\mathrm{S}^\cdot + \mathrm{S}^\cdot \xrightarrow{H^+} \mathrm{Th} + \mathrm{L}$$

Illuminated electrode

$$\mathrm{L} \longrightarrow \mathrm{Th} + 2e + 3H^+$$

Dark electrode

$$2\mathrm{Fe(III)} + 2e \longrightarrow 2\mathrm{Fe(II)}$$

where Th is

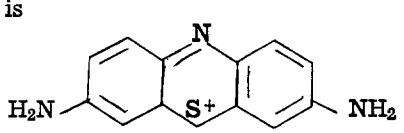

L is

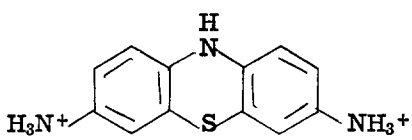

and S· is the semithionine radical.

In order to obtain power from the cell it is essential that the illuminated electrode should discriminate between the photogenerated leucothionine (L) and Fe(III) (4). If the electrode does not so discriminate, then addition of the electrode reactions in the reaction scheme shows that the electrode merely catalyzes the back-reaction of photogenerated products into the original reactants

$$\mathrm{L} + 2\mathrm{Fe(III)} \rightarrow \mathrm{Th} + 2\mathrm{Fe(II)}$$

The illuminated electrode must remove one of the photogenerated products, in this case L, and force the other, Fe(III), to diffuse across the cell and react on

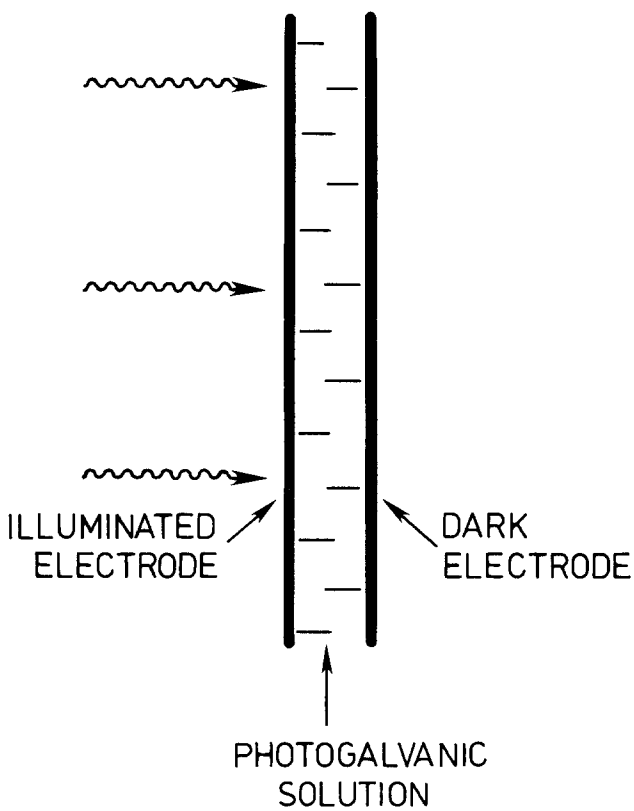

Fig. 1. Typical photogalvanic cell

Key words: photogalvanic cells, modified electrodes, thionine.